Biomaterials 30 (2009) 169–179

Contents lists available at ScienceDirect

Biomaterials

journal homepage: www.elsevier.com/locate/biomaterials

In vitro cell alignment obtained with a Schwann cell enriched microstructured nerve guide with longitudinal guidance channels

Ahmet Bozkurt [a,b,c,*], Ronald Deumens [b,d], Christina Beckmann [a], Leon Olde Damink [e], Frank Schügner [e], Ingo Heschel [e], Bernd Sellhaus [b], Joachim Weis [b], Wilhelm Jahnen-Dechent [f], Gary A. Brook [b], Norbert Pallua [a]

[a] Department of Plastic Surgery, Hand and Burn Surgery, RWTH Aachen University Hospital, Aachen, Germany
[b] Institute of Neuropathology, RWTH Aachen University Hospital, Aachen, Germany
[c] Interdisciplinary Center for Clinical Research (IZKF) BIOMAT, RWTH Aachen University Hospital, Aachen, Germany
[d] Pain Management and Research Center, Department of Anesthesiology, Academic Hospital Maastricht, Maastricht, The Netherlands
[e] Matricel GmbH, Kaiserstrasse 100, 52134 Herzogenrath, Germany
[f] Department of Biomedical Engineering, Biointerface Laboratory, RWTH Aachen University Hospital, Aachen, Germany

ARTICLE INFO

Article history:
Received 23 June 2008
Accepted 2 September 2008
Available online 14 October 2008

Keywords:
Peripheral nerve
Tissue engineering
Collagen
Cross-linking
Nerve regeneration

ABSTRACT

Therapeutic benefits of autologous nerve grafting in repair of peripheral nerve lesions have not been reached using any alternative nerve guide. Nevertheless, issues of co-morbidity and limited availability of donor nerves urgently ask for a need of bioartificial nerve guides which could either replace or complement autologous nerve grafts. It is increasingly appreciated that optimal nerve guides comprise both physical and molecular cues in support of peripheral axon regeneration. Now, we present a collagen-based microstructured 3D nerve guide containing numerous longitudinal guidance channels with dimensions resembling natural endoneurial tubes. Moreover, these nerve guides could be functionalized by Schwann cell (SC) seeding. Viable SCs did not only adhere to the nerve guide, but also migrated throughout the guidance channels. Of particular importance was the observation that SCs within the guidance channels formed cellular columns reminiscent of "Bands of Büngner", which are crucial structures in the natural process of peripheral nerve regeneration during the Wallerian degeneration. We, therefore, conclude that our orientated 3D nerve guides (decorated with SCs) with their physical and molecular properties may hold great promise in the repair of peripheral nerve lesion and serve as a basis for future experimental regeneration studies.

1. Introduction

Peripheral nerve injuries (PNI) affect about 2.8% of trauma patients [1]. A range of surgical approaches have been performed to repair even the most challenging type of PNI, i.e. neurotmesis (complete nerve transection). With nerve gaps of a few millimeters, end-to-end nerve suture repair is the preferred option. However, in cases where tension-free suture repair is not possible, a nerve bridge is required to reconnect the two nerve stumps. A variety of bridging materials have been used in experimental and occasional clinical investigations [2–4]. These materials have included natural biological tissues such as arteries, veins and muscles [5,6–8], modified biological tissues such as collagen-based and laminin-based bridges [9–11], and synthetic materials including silicon and polyesters [12–15]. Despite many advances with the majority of these materials, clinical practice still prefers the use of autologous nerve grafts [16,17]. However, this preference is greatly diminished when considering neurotmesis of multiple peripheral nerves and/or long-distance gaps, since the amount of donor material is limited and co-morbidity occurs in body parts innervated by the donor nerve(s). Over the last decades, these issues have led to a variety of studies exploring the capacities of artificial nerve guide in neurotmesis repair [18].

Artificial nerve guides ideally require functionalization for support of axonal regeneration. A number of cellular and molecular cues that are important for successful axonal regeneration have been identified during the spontaneously occurring axon regeneration response after axonotmesis injuries. Following nerve injury, regenerating axon sprouts are presented with an orientated framework of proliferating Schwann cells (SCs) in the distal nerve stump. SCs of both myelinated and unmyelinated axons multiply,

* Corresponding author. Department of Plastic Surgery, Hand and Burn Surgery, RWTH Aachen University Hospital, Pauwelsstrasse 30, 52074 Aachen, Germany. Tel.: +49 241 800; fax: +49 241 82448.
E-mail address: abozkurt@ukaachen.de (A. Bozkurt).

0142-9612/$ – see front matter © 2008 Elsevier Ltd. All rights reserved.
doi:10.1016/j.biomaterials.2008.09.017

the former resulting in formation of "Bands of Büngner", arrays of SCs and their interdigitating processes within a space circumscribed by the basement membrane ("Schwann tube") [19].

Diffusible growth factors as well as cell adhesion molecules expressed by SCs, together with the basal lamina are key players in this regeneration process [20,21]. It has become increasingly clear that the efficacy of nerve guides in supporting directional axon growth is not only determined by molecular cues, but also by physical characteristics, such as the presence of orientated pores within the nerve guide.

The purpose of the current *in vitro* study was the development of a bioartificial nerve guide mimicking autologous nerve grafts with physical properties characterized by longitudinal pore channels and chemical properties supporting the viability, proliferation and migration of SCs. Recently, in a pilot study, we could demonstrate the suitability collagen scaffolds with such of physical properties to guide neurite outgrowth from adult dorsal root ganglia [24]. Currently, for the special requirements of peripheral nerve repair with its key components (i.e. Schwann tubes and SCs), the 3D nerve guides were further improved with respect to degradation and cytocompatibility for SCs. The influence of artificial chemical cross-links on the ability of the guides to support SC adhesion, proliferation and migration was tested using a 2D model surface as well as a 3D guidance structure. At first, a 2D construct (excluding the influence of diffusion) was used to find the optimal SC and collagen scaffold combination. Subsequently, the best 2D scaffolds were chosen to fabricate 3D constructs to test the cytocompatibility of SCs with potentially impeded conditions of medium supply and nutrition associated with 3D culture conditions.

2. Materials and methods

2.1. Scaffold preparation

The scaffolds used in this study are based on the OptiMaix-2D and OptiMaix-3D scaffolds as supplied by Matricel GmbH (Herzogenrath, Germany) and were adjusted for the requirements of peripheral nerve guide tissue engineering. The purified porcine collagen is characterized by low levels of non-collagenous and non-elastin marker molecules such as cysteine (<8 μmol/g), tryptophan (<3 μmol/g) and hexosamines (<8 μmol/g) and contained 10–15% (w/w) of elastin as indicated by the presence of desmosine and isodesmosine. The 3D-collagen scaffolds with parallel oriented pores were prepared according to a patented directional freezing process (see Supplementary video 1) and the detailed preparation has been described in detail previously [24,26].

For the purpose of this study, both 2D and 3D scaffolds with varying degrees of cross-linking were prepared by cross-linking using a zero-length cross-linking method based on the use of 1-ethyl-3(3-dimethylaminopropyl)carbodiimide (EDC) (Table 1; Figs. 1 and 2) as previously described [25]. Sterility of the scaffolds was achieved by exposure to 25 kGy ^{60}Co gamma irradiation.

2.2. Degree of cross-linking

The degree of cross-linking of both the 2D as well as the 3D-collagen scaffolds was related to a decrease in free amine group content, an increase in denaturation temperature and a decrease in fluid uptake compared to non-crosslinked scaffolds (see Table 1).

The free amine group content of the samples was determined spectrophotometrically after reaction of the primary amine groups with 2,4,6-trinitrobenzenesulphonic acid (TNBS) as described previously [25]. The free amine group content was expressed as the number of free amine groups present per 1000 amino acids (n/1000 n). The percentage of reacted amine groups was calculated by setting the amine group content of the non-crosslinked sample to 100%. This value was used for sample identification as presented in Table 1.

The denaturation temperature of the scaffolds was determined by differential scanning calorimetry (DSC) using a TA Instrument Q100. In an empty hermetic pan, approximately 1 mg of scaffold was weighed, followed by the addition of 11 mg phosphate buffered saline solution. The sample was allowed to rehydrate overnight at room temperature before it was scanned at 5 °C/min in the range of 15–95 °C. Excess acid present from the directional solidification process was removed to prevent unwanted pH shifts. The peak temperature was taken as the denaturation temperature.

The fluid uptake of the 2D scaffolds was measured using culture medium. The dry weight was accurately weighed by means of an analytical balance (Sartorius™ AG, Göttingen, Germany). Every measurement was performed with $n = 4$ samples and $n = 3$ repetitions. Subsequently, the 2D scaffolds were incubated in culture medium and were cultivated in a tissue incubator at 37 °C in a humidified atmosphere containing 5% CO_2. After 1 day, the samples were weighed again and the difference between these measurements and the dry weight was used to calculate the wet/dry ratio (wet/dry ratio = $\text{weight}_{\text{in culture}}/\text{weight}_{\text{dry}}$) as an indicator for the different hydrophilic properties (e.g. swelling) as well as scaffold integrity (see Table 1).

2.3. In vitro *degradation*

The degradation of the 2D scaffolds was assessed as previously described [25] using bacterial collagenase from *Clostridium histolyticum* (EC 3.4.24.3, Sigma Chemical Company, St. Louis, MO, USA). The weight loss of the scaffolds (% w/w) was related to the hydroxyproline content released to the supernatant. The degradation rate in % w/w weight loss per hour was calculated from the linear relation between weight loss and degradation time.

A volume of 1.0 ml of 0.1 M Tris–HCl buffer (pH 7.4) containing 0.005 M $CaCl_2$ was added to a dried scaffold weighing 10 mg. After incubation at 37 °C for 1 h, 0.5 ml of a three-fold concentrated collagenase solution in Tris–HCl buffer was added to give the final intended collagenase concentration (one unit will release peptides from native collagen, equivalent in ninhydrin colour to 1.0 μmol of L-leucine in 5 h at pH 7.4 at 37 °C in the presence of calcium ions). The degradation was discontinued at the desired time interval by the addition of 0.1 ml of 0.25 methylenediaminetetraacetate (Titriplex III p.a., E. Merck, Darmstadt, Germany). Degraded samples were centrifuged for 5 min at 5000 rpm. Supernatant (0.1 ml) was added to 0.9 ml 6.6 M HCl followed by hydrolysis of collagen fragments present for 16–24 h at 95 °C. Thereafter the samples were neutralized by adding 90 μl hydrolysate to 810 μl buffer (0.125 M citric acid, 0.25 M Na_2HPO_4, containing 2.8 g NaOH per 100 ml). From this neutralized sample, 100 μl was added to 900 μl Chloramin T reagent (0.5 g Chloramin T in 100 ml 0.25 M phosphate/0.125 M citrate buffer). The sample was incubated at room temperature for 15 min. Thereafter 1800 μl Ehrlich's reagent (7 g *p*-dimethylaminobenzaldehyde in 15 ml 60% perchloric acid, made up to 100 ml with 1-propanol) was added and the sample was incubated at 75 °C for 15 min. After cooling, the absorption was measured at 570 nm using a sample not containing hydroxyproline as a blank. The hydroxyproline content was calculated using a standard curve prepared from hydroxyproline solutions with known concentrations.

2.4. Isolation of SCs

SCs were isolated from adult inbred Lewis rats (Taconic©, Lille Skensved, Denmark). All animals ($n = 10$) were maintained in accordance to the guidelines of the German animal protection statute and experimental protocols were approved by the governmental review committee. The animals (6 weeks old, average body weight 150–200 g) were housed under temperature controlled conditions at 21 ± 1 °C, with a cycle of 12 h light and 12 h darkness, with free access to food and water. SCs were expanded *in vitro* using established protocols [27,28].

After a dorsal skin incision, the sciatic nerves were exposed and resected by using microsurgical techniques. For *in vitro* degeneration, small pieces of sciatic nerves (1–2 mm) were plated on Petri dishes in standard medium consisting of Dulbecco's modified essential medium (DMEM; Invitrogen™, Karlsruhe, Germany) supplemented with 10% fetal calf serum (FCS; PAA™, Pasching, Austria) and 1%

Table 1
Characterization of cross-linking of the scaffolds developed for this study

Code	Non sterile samples			Sterile samples	
	Free amine content groups (n/1000n)	Free amine groups reacted (%)	Denaturation temperature (°C)	Denaturation temperature (°C)	Wet/dry ratio (w/w)
NX	26.6 ± 1.45	0	56.9 ± 0.5	45.8 ± 1.1	12.6 ± 0.4
17%	22.1 ± 1.35	17	67.3 ± 0.9	55.0 ± 0.7	9.4 ± 1.0
24%	20.2 ± 1.12	24	71.0 ± 0.5	nd	nd
33%	17.7 ± 1.31	33	74.2 ± 0.3	66.3 ± 0.6	7.3 ± 1.3
42%	15.3 ± 0.64	42	79.6 ± 0.6	nd	nd
57%	11.4 ± 0.24	57	84.0 ± 0.3	nd	nd

All measurements were performed $n = 3$; data is presented as mean + standard deviation. NX = non-crosslinked. nd = not determined.

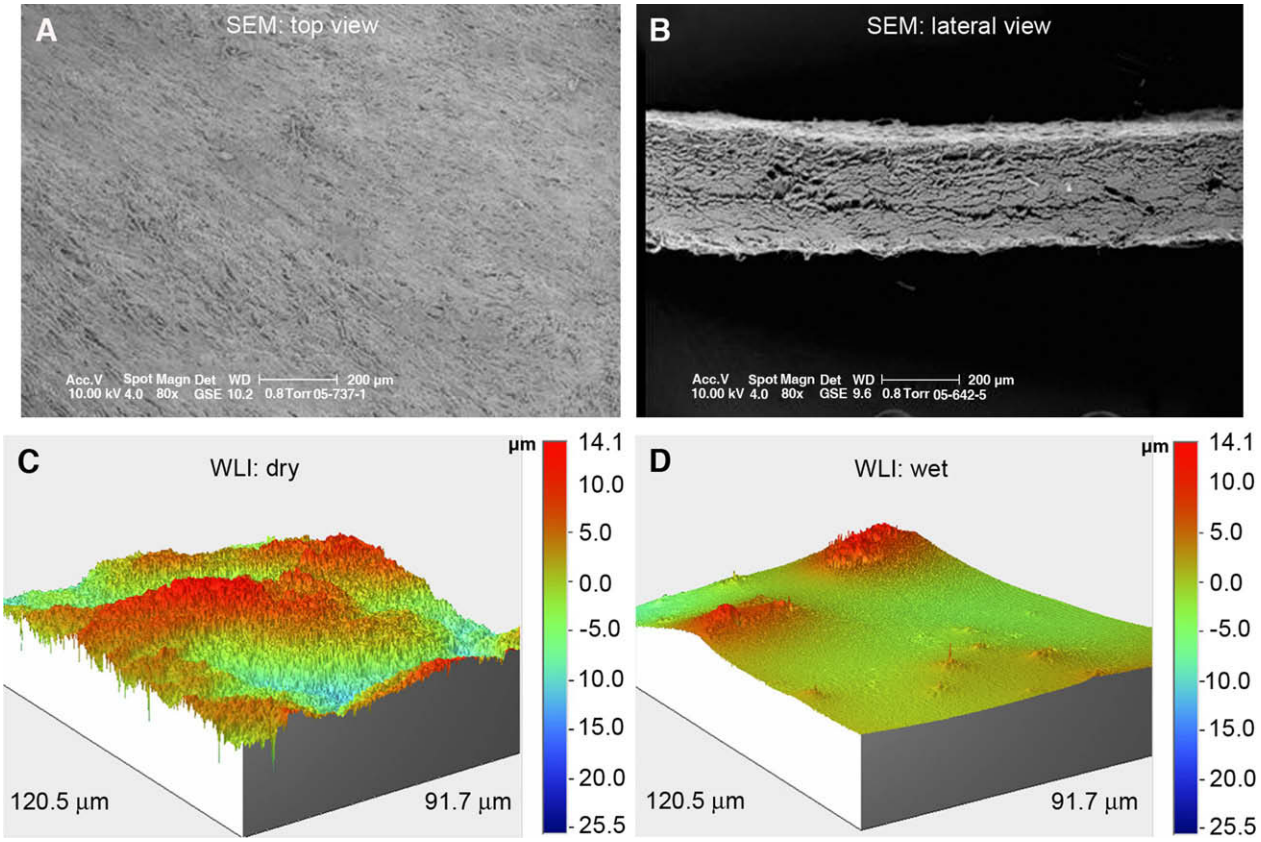

Fig. 1. Illustration of a representative 2D-collagen scaffold (i.e. 2D-33%) by means of SEM (A: top view, B: lateral view) and by means of white light interferometry (WLI) with the difference of the 2D scaffold surface in dry (C) and wet (D) conditions. After immersion into culture medium, the 2D scaffold becomes rapidly hydrated yielding an almost lane ground for seeded SCs (D).

penicillin/streptomycin (10,000 U/ml of penicillin, 10 mg/ml streptomycin; PAA™, Pasching, Austria). After 7 days of cultivation at 37 °C the sciatic nerve fragments were transferred to Falcon tubes containing collagenase (80 mg) (Collagenase C1-22, Biochrom, Berlin) and BSA (300 mg) in collagenase buffer (100 mM Hepes, 120 mM NaCl, 50 mM KCl, 1 mM $CaCl_2$, 5 mM glucose). After 2 h, 5 ml trypsin–EDTA (0.25%) were added and incubated for 1 h. The reaction was stopped by adding 1.5 ml FCS. After centrifugation, the resulting cell suspension was plated onto on poly-L-ornithine/laminin (*p*-orn/lam; both Sigma–Aldrich™, Munich, Germany) culture flasks and maintained in growth medium (179.5 ml DMEM containing 20 ml FCS, 20 mg transferrin, 8 µg bFGF, 8 µg heregulin, 40 µL 5 mM forskolin, 200 µl insulin, 200 µl gentamicin) [27,28].

2.5. Purification of SCs

To obtain highly enriched SC cultures, cell purification was performed by using the Magnetic Assisted Cell Sorting (MACS®) system (Miltenyi Biotec, Bergisch Gladbach, Germany). Flasks with unpurified cells (i.e. SCs and fibroblasts) were washed with Dulbecco's phosphate buffered saline (PBS) and incubated with trypsin (0.05%) for 5 min. The cells were collected in growth medium and centrifuged at $300 \times g$ for 5 min at 4 °C, washed with PBS supplemented with 2 mM EDTA (PE). For SC selection, unpurified cells were incubated with 2 µl of rabbit anti-mouse p75LNGFr polyclonal antibodies (undiluted Chemicon International Ltd, Hampshire, United Kingdom) in 1 ml of 95 ml Dulbecco's PBS, 2 mM EDTA, 0.5% BSA (PEB) for 10 min at 7 °C. At the end of the incubation, 500 µl of PE was added and the cells were centrifuged ($300 \times g$ for 5 min at 4 °C). Hereafter, cells were incubated with 20 µl microbead-linked rat anti-mouse IgG1 (at 1:500; Miltenyi Biotec, Bergisch Gladbach, Germany) in 80 µl PEB for 15 min at 7 °C. After two rinsing steps with PE, an MS column (Miltenyi Biotec, Bergisch Gladbach, Germany) was placed in the MiniMACS® magnet (Miltenyi Biotec, Bergisch Gladbach, Germany) and flushed with PEB. A maximum of 10×10^6 cells was resuspended in 500 µl PEB and applied onto the MS^+ column followed by three rinses with 500 µl PEB to wash out unbound cells (i.e. p75LNGFr-negative fibroblasts). After removal from the magnet, the column was flushed with 1 ml PE, which allowed to collect the p75LNGFr positive cell fraction (=SCs). The high purity (>95%) of the p75LNGFr positive cell fraction was confirmed by immunocytochemistry (Supplementary Fig. 2).

2.6. Application of cell suspensions to the collagen scaffolds

2.6.1. 2D-collagen scaffolds

Under sterile conditions, 2D-collagen scaffolds (size: 5×5 mm) were transferred into pre-moistened 24 wells (smooth side faces upwards). The SC suspensions (2500 cells/µl, total volume: 50 µl) were then loaded onto the dense fibrous surface of the 2D scaffolds. Medium was filled with caution not to shear off the SC layer on the dense fibrous surface of the 2D scaffolds. Subsequently, cell seeded 2D scaffolds were cultivated in a tissue incubator at 37 °C in a humidified atmosphere containing 5% CO_2 for a period of 3, 7 or 14 days.

2.6.2. 3D-collagen scaffolds

A volume of 25 µl of SC suspension (20,000 cells/µl) was seeded onto the 3D scaffolds (cylinder of 1 cm length and 2 mm diameter) from both ends. After this volume was fully absorbed by the scaffold, the 3D scaffold was further loaded by adding another aliquot of 25 µl of cell suspension.

To measure cell migration into the 3D scaffold (longitudinal = along the channels; horizontal = transverse/perpendicular to the channels) longitudinal cryosections of the seeded scaffold were prepared at days 3, 7 and 14 and cell nuclei were stained using the dye 4′,6-diamidino-2-phenylindole (DAPI, 1 µg/ml, 5 min).

Sections were viewed and analysed using a Zeiss Axioplan epi-fluorescence microscope connected to a Zeiss AxioVision CCD camera. Images were processed and stored using the Zeiss AxioVision 3.1 software. Using Adobe Photoshop 7 software, the distance between the lateral surface or the upper surface and the DAPI positive cell front was measured (see also Fig. 9).

2.7. Preparation of dorsal root ganglia (DRG)

Under *in vitro* conditions, 3D-cell culture experiments with SCs were used to test the ability of the longitudinal pore channels to guide neurite outgrowth from dorsal root ganglia (DRG). To this end, Lewis rats were euthanized using inhalation anaesthesia (Isofluran, Abbott GmbH, Wiesbaden, Germany) and the DRGs (containing sensory neurons, SCs and fibroblasts) were dissected from the spinal column and transferred to ice-cooled DMEM/F-12 containing 10% FCS. Using a head magnifier (Zeiss KF) and Xenon light (StarMed StarLight, Grafing, Germany), excised DRGs were divided into two halves and placed with their cut surface directly onto the surface of the 3D scaffold (e.g. Fig. 6). The ganglia were positioned such that

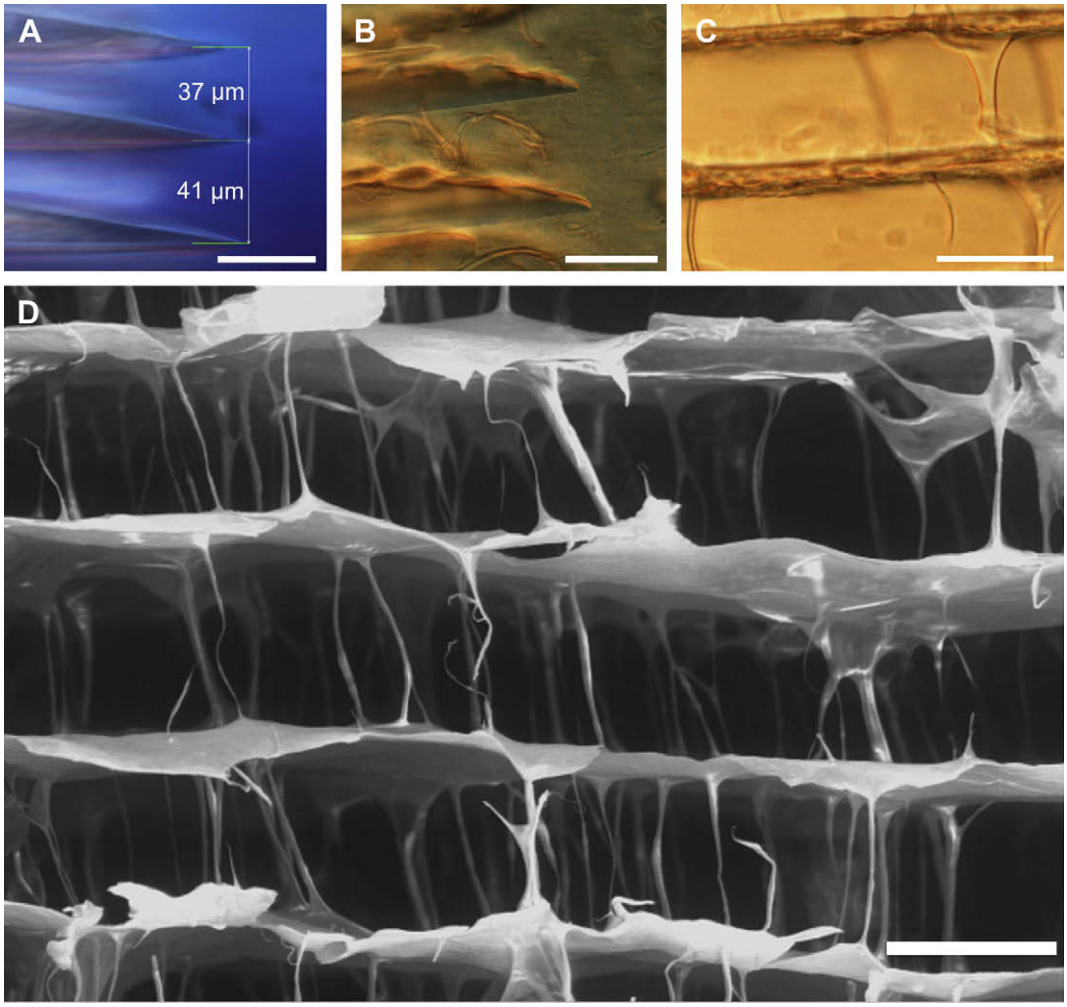

Fig. 2. Micrographs of finger-like ice crystals extending uniformly through a pure crystalline solution (A) or collagen dispersion (B). During the patented freeze-drying process, the collagen is concentrated between the finger-shaped ice crystals, thereby forming the walls of the oriented channels (B, C). Orientated 3D scaffolds viewed by SEM (D). The presented nerve guide concept is characterized by its high degree of porosity, and more importantly, a remarkable degree of orientation with pore sizes between 20 and 50 µm. (A–D: scale bar = 50 µm).

neural and non-neural elements could penetrate the open ends of the longitudinal channels. DRG-loaded 3D scaffolds were then transferred to Petri dishes which were maintained in a tissue culture incubator at 37 °C in a humidified atmosphere containing 5% CO_2.

2.8. Immunocytochemistry

After 21 days in culture, SCs in culture flasks and scaffolds with SCs or DRGs were fixed for 60 min in 4% paraformaldehyde (PFA) in 0.1 M PBS (4 °C) and processed for immunocytochemistry (Figs. 6 and 7; Supplementary Figs. 2 and 3).

Longitudinal sections (50 µm thickness) of 3D scaffolds (loaded with either SCs or DRGs) were prepared using a cryostat and then mounted and dried onto SuperFrost Plus Gold glass slides (Menzel-Glazer, GmbH, Braunschweig, Germany). After a washing step of 3 × 5 min with HBSS, non-specific antigens were blocked with 3% normal goat serum (Sigma, Munich, Germany) and 1% Triton ABD (antibody diluent) for 60 min.

Sections with DRGs (see Section 2.4) were then incubated overnight using the following primary antibodies: monoclonal anti-neurofilament 200 kDa (NF200; clone NE14, 1:5000, Sigma), monoclonal anti-vimentin (clone V9, 1:20,000, Sigma) or polyclonal anti-S100 (1:1000, Dako). The sections were then further processed for either peroxidase staining or double immunofluorescence. For peroxidase staining, following extensive rinsing steps in 0.1 M PBS, sections were incubated in biotinylated goat anti-mouse or goat anti-rabbit antibody (Vector Laboratories, diluted 1:500) for 1 h at room temperature. This was followed by the Vector ABC (Standard kit, Vector Laboratories) system and subsequent 5 min incubation in diaminobenzidine for visualization of the reaction product.

3D scaffolds with SCs as well as six-wells with SCs (see 2.3.2) were incubated overnight using the following primary antibodies: monoclonal anti-vimentin (clone V9, 1:20,000, Sigma), monoclonal anti-nestin (Chemicon, 1:2000), or polyclonal anti-S100 (1:1000, Dako), polyclonal anti-GFAP (1:2500, Dako), polyclonal anti-p75 (1:2000, Chemicon). For immunofluorescence, following washing stages, specimens were incubated in a mixture of Alexa-488 conjugated goat anti-rabbit and Alexa-594 conjugated goat anti-mouse antibody (both 1:500, Molecular Probes, Paisley, United Kingdom) at room temperature for 3 h. Counterstaining was conducted using the nuclear dye 4′,6-diamidino-2-phenylindole (DAPI, 1 µg/ml, 5 min).

2.9. XTT proliferation

Cell viability and proliferation was determined by using the Cell Proliferation kit II (Roche Applied Science, Mannheim, Germany) (Fig. 5).

In brief, cell seeded 2D scaffolds in 24 wells were cultivated for periods of 1, 3, 7 and 14 days. At these specific time points, the culture medium in the 24-well plates was replaced by a solution containing 250 µl XTT labelling reagent and 500 µl culture medium. Then, the wells were incubated for 4 h in a tissue culture incubator at 37 °C in a humidified atmosphere containing 5% CO_2. After this 4-h incubation time, spectrophotometric absorbance of the formazan dye in supernatant (each 100 µl in a in a 96-well plate) was read by an enzyme-linked immunosorbent assay (ELISA) reader at a wavelength of 492 nm with a reference point at 690 nm. Negative control experiments were performed by means of cell-free collagen scaffolds.

2.10. Scanning electron microscopy (SEM)

Samples of SC loaded 2D and 3D scaffolds were also processed for SEM (Figs. 4 and 8). The scaffolds were fixed for 24 h in 4% glutaraldehyde in 0.1 M PBS. After dehydration in acetone using a Polaron E3000 critical point dryer (Polaron Equipment Ltd., Watford, United Kingdom), the specimens were mounted on stubs and sputter coated with gold, loaded into an ESEM XL30 FEG scanning electron microscope (Philips EO, Eindhoven, NL), and viewed under an accelerating voltage of 5 kV.

2.11. White light interferometry (WLI)

WLI measurements were performed using a Wyko NT2000 white light interferometer (Veeco, GB). The operating principle of this instrument is the interference pattern formed by a reference and a specimen beam with path difference, which is described elsewhere [29]. A light beam from a tungsten halogen lamp is split by an objective lens. One of the beams is focused onto the specimen surface and another onto an inner reference plane. After reflection, the two beams are superimposed one to another in the interferometer. By accurate vertical scanning, produced by a piezo electrical measurement converter (PZT), and a camera able to measure the intensity of the individual pixels, a 3D interferogram of the surface is produced. A quantitative 3D-image is then produced from computer calculations by Frequency Domain Analysis (Fig. 1).

2.12. Statistical analysis

Statistical examinations of metabolic activities (Fig. 5), cell migrations (Fig. 9) and medium uptake (wet/dry ratio; Table 1) were tested using standard analysis of variance (ANOVA; SPSS 10, SPSS Inc., Chicago, IL, USA) with Bonferroni post hoc correction for multiple corrections. A p value of 0.05 was regarded as the level of significance.

3. Results

3.1. Scaffolds

The following pictures show examples of the developed and tested 2D and 3D-collagen scaffolds (Figs. 1 and 2). The scaffolds were produced using a top down freezing procedure illustrated in Supplementary video 1.

The characterization of the scaffolds used in this study is presented in Table 1. Cross-linking using EDC involves the activation of carboxylic acid groups followed by reaction with free amine groups (25), resulting in a decrease in free amine group content and an increase in thermal stability (denaturation temperature) when compared to non-crosslinked scaffolds. No significant differences in changes in free amine group content or thermal stability were observed when either 2D or 3D scaffolds were crosslinked. Based on the percentage of free amine groups that had been reacted and crosslinked, a number of scaffolds presenting different extents of cross-linking (2D: 17–57% or 3D: 17–57%) were generated and tested. Gamma sterilization induced a decrease in denaturation temperature for the scaffolds investigated, but did not induce a significant change in free amine group content (data not shown in Table 1).

Regarding the hydrophilic properties, 2D non-crosslinked (NX) scaffolds showed the highest culture medium uptake (wet/dry ratio of 12) followed by 2D-17% (wet/dry ration of 9) and 2D-33% the lowest medium uptake (wet/dry ratio of 7).

3.2. Influence of cross-linking on in vitro degradation

To investigate the effect for the degree of cross-linking on the resistance towards degradation, 2D scaffolds were exposed to bacterial collagenase and the resulting weight loss was monitored as a function of degradation time. From the linear relation observed between weight loss and degradation time, the rate of weight loss expressed as % weight loss per hour was calculated.

In a first experiment, the 2D scaffold with a denaturation temperature of 71.0 °C (2D-24%) was exposed to different concentrations of bacterial collagenase (100 IU/ml, 200 IU/ml, 300 IU/ml, 600 IU/ml and 1000 IU/ml) and the rate of weight loss was measured as described above. The results of these experiments are presented in Supplementary Fig. 1. A linear increase in degradation rate was found for collagenase concentrations up to 600 IU/ml. Increase of the collagenase concentration up to 1000 IU/ml only resulted in a limited increase of the rate of weight loss.

Based on the results in Supplementary Fig. 1, a collagenase concentration of 600 IU/ml was selected to study the influence of different degrees of cross-linking on the degradation rate. The results of these experiments are presented in Fig. 3. Thus, a decrease in degradation rate for increasing degree of cross-linking was found, indicating that control of the degree of cross-linking is an effective tool for controlling the susceptibility of collagen scaffolds to degradation.

3.3. SC culturing

For validity and reliability of the 2D and 3D scaffold experiments, tissue culture experiments on PLL-laminin-coated Petri dishes were used to verify and characterize that SC populations were highly enriched.

Prior to cell seeding experiments, random samples of the SC cultures were characterized by a series of antibodies. Double immunofluorescence with antibodies against specific and unspecific glial cell markers (i.e. S100, nestin, GFAP, p75, vimentin) proved the high cell purity and cell vitality of primary SC cultures used for seeding experiments (Supplementary Fig. 2). Primary cultures revealed highly viable SC numbers displaying typical morphology with spindle-shaped bodies and (tri-) bipolar processes (Supplementary Fig. 2). In contrast to only rare contaminating fibroblasts, SCs were strongly immunopositive for S100, GFAP, p75 and nestin (Supplementary Fig. 2).

3.4. 2D scaffolds: cytocompatibility

Based on the results of the *in vitro* degradation study, the 2D-17% and 2D-33% scaffolds were selected to perform the cytocompatibility experiments. 2D-NX scaffolds were used as control materials not exposed to cross-linking agents.

As a quantitative indication for cell proliferation on the 2D scaffolds, mitochondrial metabolic activity was measured using the XTT-proliferation assay (Fig. 5). Until day 3, only reduced metabolic activities with mean values only a little above control levels could be measured with average values between 0.195 ± 0.039 and 0.260 ± 0.037 (mean $\pm$ sem). By day 7, metabolic activity increased rapidly with absorbance values ranging between 0.204 ± 0.041 and 0.332 ± 0.047. By 14 days, the highest activity could be detected with the 2D-NX scaffold (day 14: 0.545 ± 0.070) followed 2D-17% scaffold (day 14: 0.498 ± 0.091) and 2D-33% scaffold (day 14: 0.456 ± 0.041) (Fig. 5).

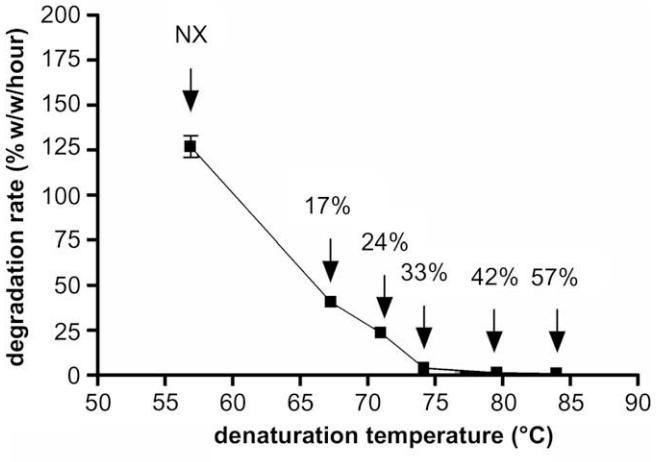

Fig. 3. Degradation rate as a function of denaturation temperature (see also Table 1). For this experiment, scaffolds with the following degree of cross-linking were used: 2D-NX, 2D-17%, 2D-24%, 2D-33%, 2D-42% and 2D-57%. Results are expressed as average + standard deviation, $n = 3$.

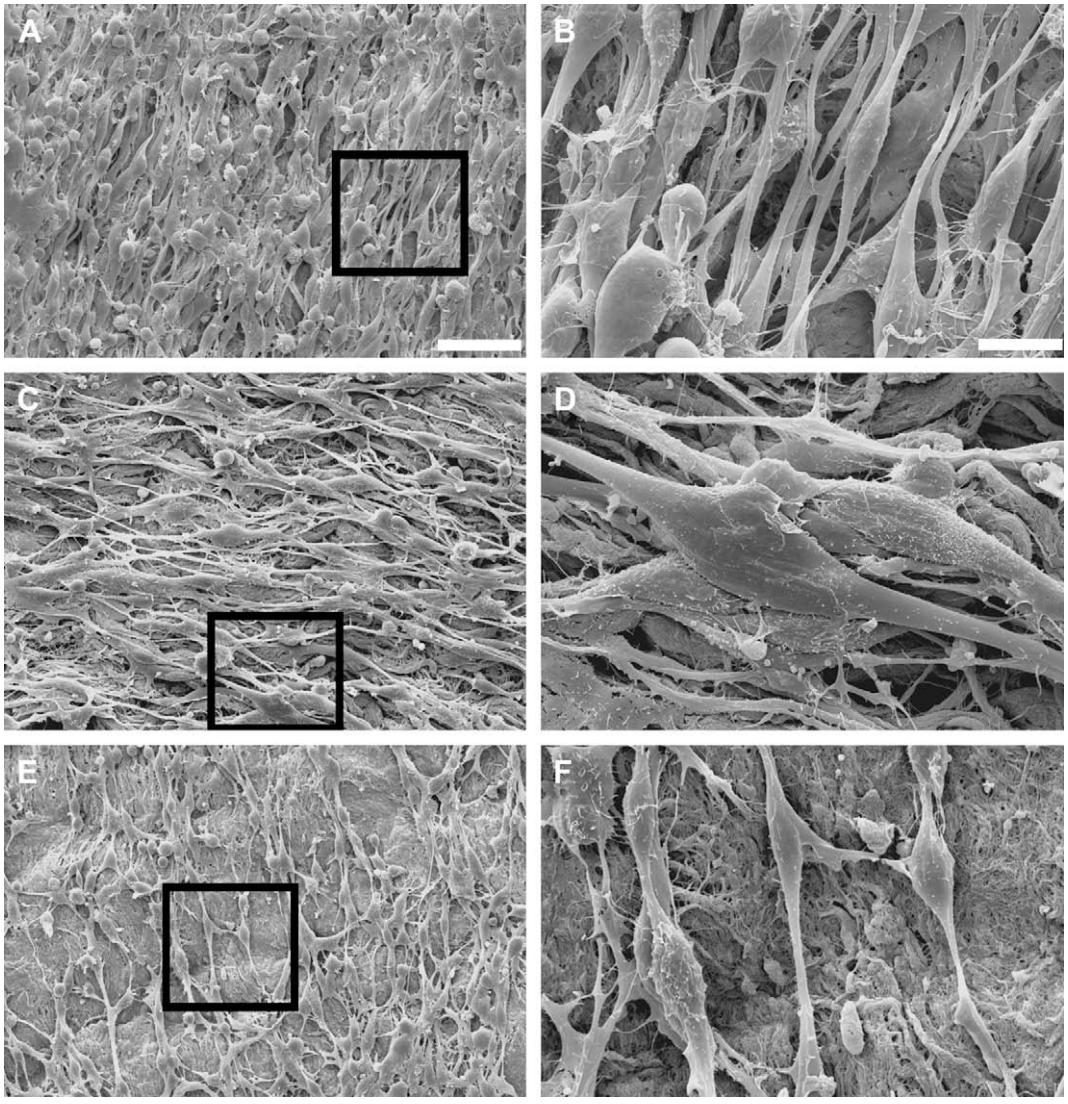

Fig. 4. High magnification SEM of SCs seeded onto 2D scaffolds (A–B: NX-2D scaffold; C–D: 17%-2D scaffold; E–F: 33%-2D scaffold) after 14 days of cultivation. Note morphological criteria for SC vitality with oval-round cell bodies and elongated cell processes. (A, C, E: scale bar = 50 μm; B, D, F scale bar = 10 μm).

For both 2D-NX scaffold and 2D-33% or 2D-17% scaffolds, there was a statistically significant metabolic increase over the observation period of 14 days (day 1, 3, 7 vs. 14: $p < 0.01$). At each time point, except at day 7 (2D-33% vs. 2D-17% scaffolds: $p < 0.01$), there was no statistically significant higher SC metabolic activity with 2D-NX scaffolds compared with 2D-33% and 2D-17% scaffolds 2D scaffolds ($p > 0.05$).

As illustrated (Fig. 4), SCs adhered well on the 2D scaffolds maintaining a high vitality and typical SC morphology with elongated processes, oval-rounded cells bodies and a high number of cell–cell contacts.

3.5. *3D scaffolds:* in vitro *regeneration*

In vitro regeneration experiments with DRGs were performed in order to test whether the longitudinal channels remain open and continuous and served as guidance cues both for SCs and neurites.

DRGs were hemisected and were loaded with their cut surface in direction to the longitudinal guidance channels (Fig. 6). The explants adhered to the surface of the scaffold. Cell migration into the scaffold became apparent supporting axonal growth derived from DRG sensory neurons. Immunocytochemistry of the DRG-

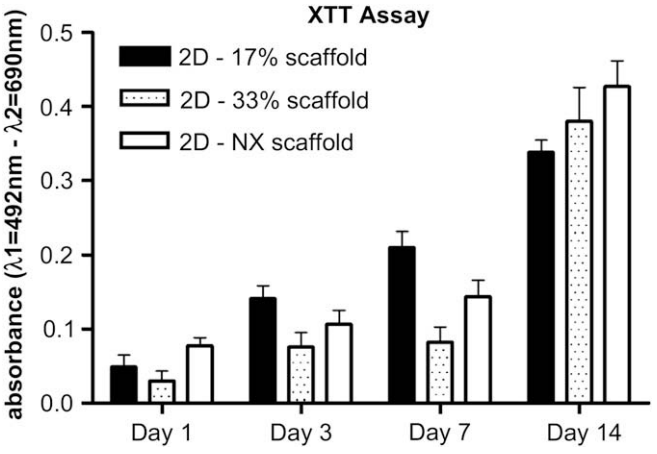

Fig. 5. Metabolic activity of SCs after seeding onto 2D scaffolds. At day 14, there was no statistical significant difference between the crosslinked (2D-17% and 2D-33% scaffolds) and non-crosslinked (2D-NX scaffold) samples.

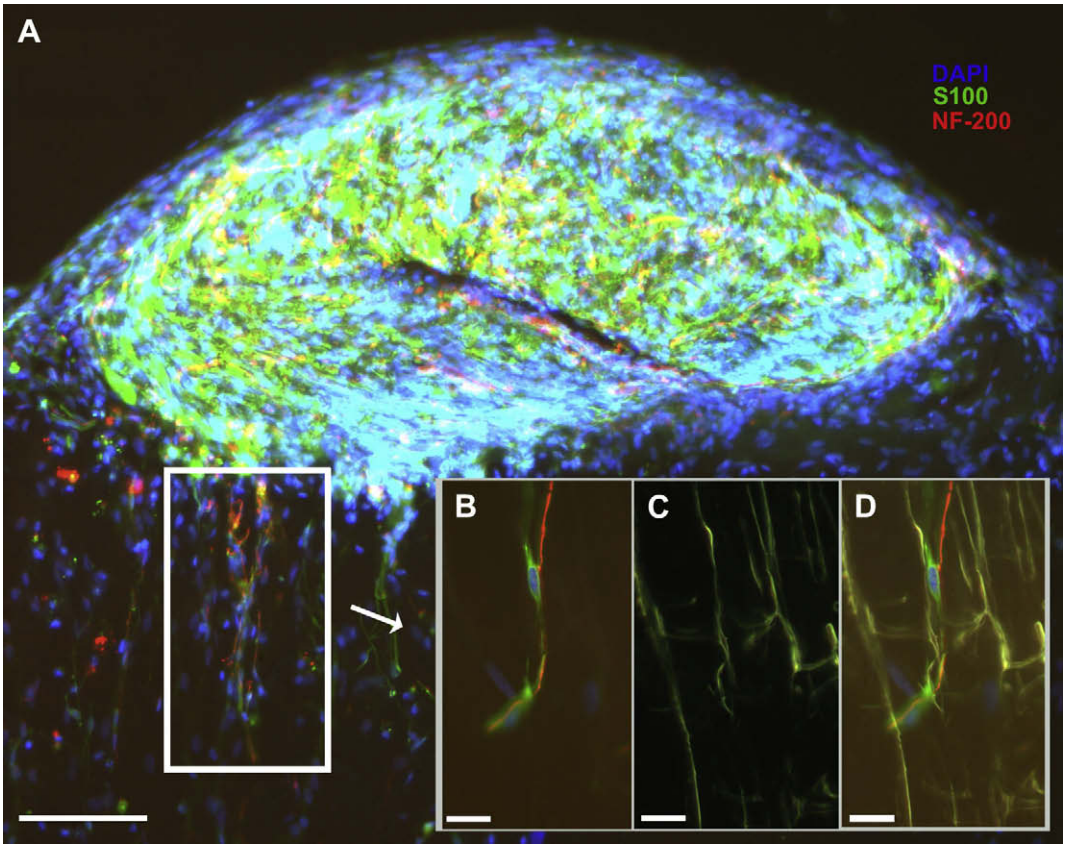

Fig. 6. Immunocytochemistry after 14 days of cultivation. Illustration of a hemisected DRG loaded onto 3D scaffold (A). Neurofilament staining revealing the close association between regenerating axons (=red) and migrating SCs (B) (S100 = green; DAPI = blue). Illustration of the microstructure with longitudinal channels for mechanical stability (C). By superposition of Fig. 6B and C the orientation of SCs supporting growing axons within the longitudinal channels can be identified (D). (A: scale bar = 100 μm; B–D: scale bar = 20 μm).

loaded scaffolds revealed densely packed SCs and fibroblasts within the hemisected capsule of the ganglion (Fig. 6A). These cells migrated into the scaffold, either as individual cells in a scattered fashion (mainly fibroblasts; S100-negative) or as bundled cells in a columnar fashion (mainly SCs; S100-positive). The latter displayed a longitudinal arrangement (Fig. 6B) within the predetermined scaffold channels (Fig. 6C and D). Double immunofluorescence was used to demonstrate the spatial relationship between the migrating cells and axons (NF200-positive) (Fig. 6B). Neurofilament immunocytochemistry showed that axons were arranged in groups within the channels and were closely associated with the columns of orientated migrated SCs.

3.6. 3D scaffolds: cytocompatibility

To support significant axonal growth over critical distances under *in vivo* conditions, the presence of numerous, highly viable and orientated SCs is indispensable. Although the 2D investigations demonstrated that there was no effect of the degree of cross-linking on SC viability and proliferation, it was necessary to fabricate 3D scaffolds to assess this property under conditions where cells are deeply embedded within a microstructured 3D scaffold.

After seeding of the 3D scaffolds with SCs, immunocytochemistry demonstrated the orientation and typical morphology of SCs and their processes in parallel with the longitudinal guidance channels keeping their typical cell morphology (Fig. 7; Supplementary Fig. 3). After seeding of the scaffolds, SCs rapidly attached to the collagen surface. The cells extended long processes and migrated into the collagen scaffold, which became thoroughly colonized by the SCs within two weeks. The morphology of the cells remained stable for at least 14 days, even as they migrated deep into the collagen scaffold and arranged themselves in a columnar fashion along the guidance pores. Fig. 7 illustrates that the columnar grouping of the SCs resembled the "Bands of Büngner" a typical feature of Wallerian degeneration.

Concerning *cell migration*, SCs migrated deep into the collagen scaffold and demonstrated a homogeneous and dense cell pattern with a parallel and longitudinal orientation along the channels indicating that the SCs followed to the tubular collagen structure (Figs. 7 and 8; Supplementary Fig. 3). It is worth noting that there was also substantial migration in the horizontal direction (=perpendicular to the main longitudinal axis of the pores). Fig. 9 shows the quantitative analysis of both longitudinal and horizontal cell migrations. In the longitudinal direction (i.e. along the longitudinal pores) 3D-17% and 3D-33% scaffolds supported migration distances of 1492 ± 459 μm and 1533 ± 130 μm, respectively, over 14 days. For both collagen modifications, SC migration along the longitudinal channels was statistically significantly increased after 14 days (day 3 vs. day 14: $p < 0.01$). There was no statistically significant difference between 3D-17% and 3D-33% scaffolds. In the horizontal direction, the initial penetration after day 3 showed no statistically significant difference with the data at 14 days ($p > 0.05$).

4. Discussion

The present study described a newly developed collagen-based 3D scaffold, which is highly porous reminiscent of "Schwann tubes" and which can be effectively seeded with SCs. Upon seeding onto the scaffold, SCs do not only migrate throughout the scaffold, but also

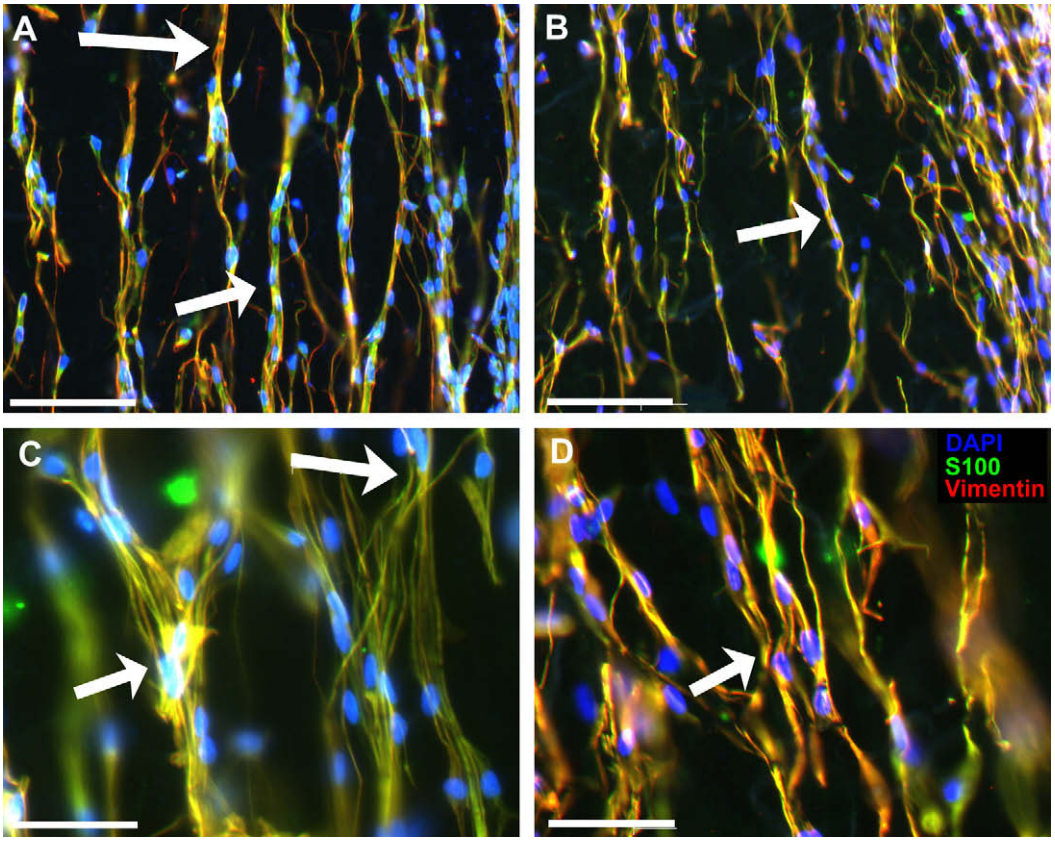

Fig. 7. Immunocytochemistry of SCs within the 3D-collagen scaffolds after 14 days (blue = DAPI, red = vimentin, green = S100). Note the arrangement of SCs in a columnar fashion along the guidance pores resembling "Bands of Büngner" (white arrows) in 3D-17% scaffolds (A, C) and in 3D-33% scaffolds (B, D). (A, B: scale bar = 100 μm; C, D: scale bar = 50 μm).

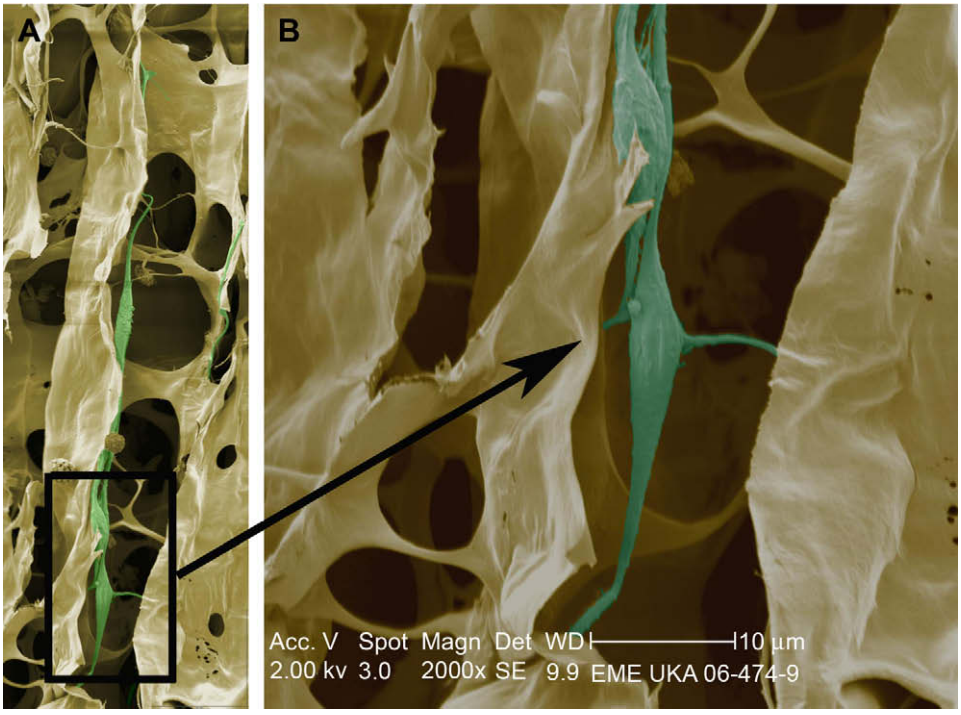

Fig. 8. A colour-modified SEM (green = SC, ochre = scaffold) picture displaying the orientation of SCs within the longitudinal guidance channels after 14 days. SCs in (B) are part of SC columns (A) with characteristic morphology resembling bands of Büngner.

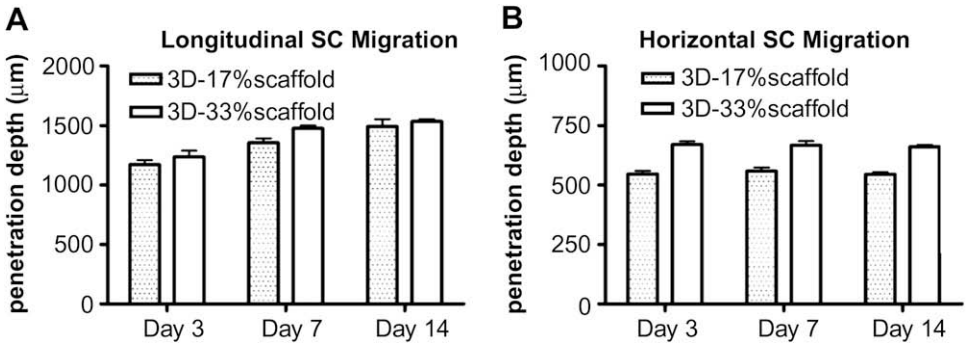

Fig. 9. Migration of SCs after cell seeding along the longitudinal (A) and horizontal axes (B).

give rise to longitudinally arranged columns. These resemble the columns of SCs ("Bands of Büngner") which are observable in the distal stump after peripheral nerve injury during Wallerian degeneration. SC seeding may provide the collagen scaffold with optimal features regarding support of axonal regeneration as it can functionalize the scaffold with a multitude of molecular factors. These can also be found in autologous nerve grafts, which are regarded as the gold standard in repair of peripheral nerve defects [34].

Decades of investigations on peripheral nerve repair strategies have demonstrated that both molecular and physical cues are essential to obtain significant regeneration of injured peripheral axons across nerve gaps. Many of the molecular and physical cues needed have been identified in studies on crush injuries (i.e. axonotmesis) in which injured peripheral axons face spontaneously aligned bundles of SCs ("Bands of Büngner") within the preserved "Schwann tubes" of the endoneurium [47,48]. These "Bands of Büngner" are formed after a highly proliferative SC response elicited by the loss of SC–axon contacts upon axon injury [54]. The orientated SC bodies and processes, which give rise to the "Bands of Büngner", are then used by injured axons [55] which regrow all the way to their target [56]. Notably, this axon regrowth occurs within the "Schwann tube" lining the "Bands of Büngner". For this reason, SCs are likely the optimal cell population to be used in repair approaches for peripheral nerve injury repair [57–60]. However, besides a crucial role for the SCs *per se*, also the intact "Schwann tubes" may be involved in the successful axon regeneration after peripheral nerve crush. Indeed, when aligned and columnar SCs were formed within the tubes of acellularized (gracilis) muscle, this improved peripheral nerve regeneration [33]. The fact that a framework of both "Schwann tubes" and "Bands of Büngner" are indispensable in effective peripheral nerve regeneration may underlie the gold standard status of autologous nerve grafting in repair of peripheral nerve gaps, which are too large to allow tension-free suture repair. However, issues like co-morbidity and limited donor tissue cast a marked shadow over the otherwise beneficial autologous nerve grafts, and thereby elicited a surge in the development of alternative repair approaches.

Up to date, no alternative approach to autologous nerve grafting (e.g. sural nerve) has demonstrated a higher or even similar degree of functional benefit. The effect of physical and molecular cues has been extensively investigated [30], but there is currently no synthetic nerve guide that possesses properties that closely resemble those of autologous nerve transplants. Clinically, empty nerve guides have thus far been approved and applied for human use including hydrogel, collagen, and polyglycolic-acid tubes [2–4]. However, entubulization of the proximal and caudal stumps using empty conduits has only provided limited guidance to bridge small nerve gaps. Long-distance regeneration of severed peripheral axons across neurotmesis gaps, on the other hand, requires a bridging approach which entails molecular and physical cues [31,32].

The present *in vitro* investigation focuses on the use of type I collagen. Despite the fact that collagen type I (typical for the epineurium) is used instead of type III (typical for the endoneurium), it could be demonstrated that this ECM protein can be engineered into a 3D scaffold with numerous microstructured guidance channels, effectively mimicking the "Schwann tubes". The high degree of porosity and, more importantly, a remarkable degree of orientation, with channel sizes between 20 and 50 μm, characterizes the present nerve guide (Fig. 2). Importantly, these nerve guide characteristics mimic the natural nerve. Physical features are characterized by the enkapsis of the peripheral nerve (Schwann tube → endoneurium → perineurium → epineurium). In myelinated nerve fibers, the SCs are arranged in a longitudinal sequence along the axon's surface and meet each other at the "Nodes of Ranvier". Further detailed, the axon is surrounded by concentric layers of SCs' cytoplasm and myelin, which are bound peripherally by a continuous basal lamina. This basal lamina, together with the endoneurial reticular and collagen fibers, provide the framework supporting the nerve fiber and are called "Schwann tube", which are longitudinal and continuous [37]. The diameters of these "Schwann tubes" are mainly defined by the axon diameters, which, regarding group A nerve fibers, ranges between 2 and 5 μm ($A\delta$) and 15 and 20 μm ($A\alpha$). As one advantage of the used patented "unidirectional freezing" process followed by freeze-drying [24,26] resulting in continuous and longitudinal orientated guidance channels, the pore diameter can be adjusted to the particular requirements with a high reproducibility. We, therefore, chose customized pore size ranging between 20 and 50 μm (mean ± SD: 33.46 ± 6.7 μm) (Fig. 2). Furthermore, our chosen pore size is not only in agreement with the (sub-) microscopical dimension of the natural "Schwann tube", as described above, but also in agreement with a variety of studies. For example, Lietz and colleagues [38] used an innovative nerve guide on the basis of a poly-trimethylene carbonate-*e*-caprolactone (TMC-CL) tube with an inner framework consisting of poly-glycolide (PGA) filaments, which were precoated with poly-D-lysine (PDL)/laminin and seeded with SCs. It was reported that longitudinally orientated micro-grooves were essential for the orientation of SC processes and axonal growth from embryonic chicken DRG. Non-orientated samples resulted only in random and irregular SC alignment and a meandering pattern of axonal growth [38]. Despite differences in the composition of the scaffold (i.e. TMC-CL and PGA vs. type collagen) both concepts follow a similar theme: mimicking to some extent the orientated architecture of an autologous nerve graft. The pore size of the collagen scaffold (20–50 μm) and the microstructured PGA filaments within the TMC-CL conduit both had similar effects in controlling the direction of glial and axonal growth. Interestingly, lane widths larger than 50 or 100 μm were reported to induce much less control of SC orientation [38]. Likewise, a recent report in which micro-patterned groove widths of approximately 30 mm

were reported to exert the most influence over the orientation of neurite growth (channel widths that were tested ranging from 30 to 1000 mm) supports this notion [39]. A further study [40] examined the neurite growth from PC12 cells, which were seeded onto micro-patterned and collagen-coated surfaces with microchannels. Channel width ranged between 20 and 60 μm. It could be shown that microchannels of 20–30 μm width were most useful to direct the growth of the neurons.

In the present investigation, collagen was used to fabricate the nerve guides. Collagen represents the most abundantly expressed ECM molecule. It is present in large amounts in specialized ECM mats along the endoneurial tubes: the basal lamina. Moreover, collagen is highly versatile for tissue engineering. Its structural stability and resorption rate can be modified by a number of cross-linking strategies [36,41–44]. Therefore, collagen has been widely used already in the fabrication of guides for peripheral nerve repair. Collagen type I gels were used to bridge a complete 2-cm-long defect of the tibial nerve. This approach did not result in the presence of myelinated axons at the distal end of the guide after eight weeks [22,23]. However, when collagen fibers were created with diameters of 100–150 μm and were inserted into 15 mm-long silicon tubes and used to bridge completely transected tibial and sciatic nerves, myelinated axons were observed at the distal end of the guides [23]. Even more impressive were the findings with novel collagen fibers with a 20-μm diameter which were arranged in bundles to create collagen fiber guidance tubes. The number of myelinated axons found at the distal end of 22 mm guides inserted into sciatic resection gaps were equal to those found after autologous nerve grafting [23]. These and other data once again indicated that not only the molecular composition of a nerve guide, but also its structural characteristics play a key role in the support of peripheral axon regrowth [35,45].

Cross-linking of collagen has been extensively used in biomaterial engineering to prevent collagen degradation. In order to prevent cytotoxic effects of cross-linking agents, previous substances like glutaraldehyde were replaced by cross-linking agents like EDC/NHS [25]. In the 2D experiments, it was demonstrated that the degree of chemical cross-linking had no direct effect on the SC metabolic activity since there was no statistical significant difference between the NX-2D scaffolds on the one hand and the 17% or 33%-2D scaffolds (Fig. 5). Optimally, the nerve guide should degrade by the time that regenerating axons reach the distal nerve segment [46]. An adverse effect would be degradation or loss of structural integrity before axonal re-innervation of target tissues. This is a major advantage of future collagen-based nerve guides. Since neurotmesis injuries range from gaps of a few millimeters (e.g. proper digital nerves) to gaps of more than 10 or 15 cm (e.g. brachial plexus lesions or cross facial nerve transfers), the degree of degradation can be adjusted to the particular injury. For example, fast degradation for collagen scaffolds in small nerve gaps or slow degradation in cases of large defects. Also 3D experiments confirmed that zero-length cross-linking with EDC did not hamper SC viability, proliferation or migration. Of utmost importance to future neurotmesis-repair approaches, these novel scaffolds could be efficiently seeded with SCs (Figs. 7 and 8; Supplementary Fig. 3). SCs, deep within the 3D scaffold, remained viable (Fig. 7). Numerous SCs migrated far into the aligned pores and formed bundles, both in the horizontal (Supplementary Fig. 3E and F) and in the vertical direction (Supplementary Fig. 3A–D). Since the typical diameter of transplanted autologous nerves range (depending on the patient's constitution) between 1 and 2 mm, a horizontal migration of 750 μm from both sides (=1.5 mm) (Fig. 9B) would ensure a sufficient cell loading and diffusion barrier. The SCs adopted a columnar arrangement (Figs. 7 and 8), highly reminiscent of the "Bands of Büngner" [19]. Results of other groups suggested that scaffolds with "Schwann tube"-like structures may be required to promote adequate and substantial nerve regeneration [35,36]. In agreement with this suggestion, we observed a spatial relationship between migrating SC and NF200-positive neurites of DRG sensory neurons. Using neurofilament immunocytochemistry we showed that the neurites were arranged in groups within the channels and were closely associated with the columns of orientated migrated SCs.

In our view, the present collagen-based microstructured nerve guide with longitudinal guidance channels combined with SC seeding provides an optimal tool for repair of peripheral nerve gaps. Artificial nerve guides require functionalization, i.e. biological signals that elicit and/or enhance peripheral axon regeneration. SCs are of utmost value in this respect, because they have a natural tendency to spontaneously align themselves in cellular bundles [48], but also have a molecular profile beneficial to peripheral nerve regeneration. Not only do SCs form a basal lamina, but they also express cell adhesion molecules important for axon growth including N-CAM, L1, and N-cadherin [49–51]. Moreover, SCs express a wide range of diffusible growth promoting factors such as NGF, BDNF, FGF-2, and CNTF [50,52,53].

5. Conclusion

The novel, highly porous, orientated collagen-based conduit described here meets at least three important criteria for neurotmesis repair. First, the conduits have appropriate chemical characteristics, i.e. collagen-based nerve guides have been proven feasible in a variety of biomedical applications. Second, on a structural level, these nerve guides consist of numerous interconnected pores, which allow for directional regeneration of axons. Third, these conduits can be functionalised by pre-seeding them with SCs. The spontaneous alignment of seeded SCs in bundles throughout the collagen scaffolds suggests the presence of a glial framework highly supportive of peripheral nerve regeneration. Future studies are now designed to show the beneficial use of these nerve guides *in vivo* and address their potential as an alternative or complementary repair strategy to autologous nerve grafts.

Acknowledgements

The authors are indebted to PD Dr. Franz Lassner (Praxisklinik am Boxgraben, Aachen, Germany) for his permanent support and enthusiastic commitment. The authors thank Julian Tank, Dr. Michael Wöltje and Dr. Sven Möllers for helpful comments in biological and technical questions. The authors thank Dr. Jochen Salber for providing the WLI and Dr. Lizette Eummelen for her help with the XTT test. A. Bozkurt was supported by grants #0312758, #0315140, #0313640 from the Federal Ministry of Education and Research (BMBF) and by grants ("START" program) and research fellowship ("START-Rotation") provided by the Faculty of Medicine of the RWTH Aachen University of Technology. G. Brook was supported by funds of the German Aerospace Center (DLR; 01GN0109). R. Deumens was supported by KNAW-Hendrik Casimir Karl Ziegler Research Stipend and KNAW-van Leersum Fund.

Appendix. Supplementary data

Supplementary data associated with this article can be found in the online version, at doi:10.1016/j.biomaterials.2008.09.017.

Appendix A

Figures with essential colour discrimination. Certain figures in this article, especially Figs. 1, 2, 6, 7 and 8 are difficult to interpret in black and white. The full colour images can be found in the on-line version, at doi:10.1016/j.biomaterials.2008.09.017.

References

[1] Noble J, Munro CA, Prasad VS, Midha R. Analysis of upper and lower extremity peripheral nerve injuries in a population of patients with multiple injuries. J Trauma 1998;45(1):116–22.
[2] Meek MF, Coert JH. Clinical use of nerve conduits in peripheral-nerve repair: review of the literature. J Reconstr Microsurg 2002;18(2):97–109.
[3] Meek MF, Coert JH. US Food and Drug Administration/Conformit Europe-approved absorbable nerve conduits for clinical repair of peripheral and cranial nerves. Ann Plast Surg 2008;60(4):466–72.
[4] Schlosshauer B, Dreesmann L, Schaller HE, Sinis N. Synthetic nerve guide implants in humans: a comprehensive survey. Neurosurgery 2006;59(4):740–7. Discussion 7–8.
[5] Walton RL, Brown RE, Matory Jr WE, Borah GL, Dolph JL. Autogenous vein graft repair of digital nerve defects in the finger: a retrospective clinical study. Plast Reconstr Surg 1989;84(6):944–9. Discussion 50–52.
[6] Tang JB, Shi D, Zhou H. Vein conduits for repair of nerves with a prolonged gap or in unfavourable conditions: an analysis of three failed cases. Microsurgery 1995;16(3):133–7.
[7] Tang JB. Vein conduits with interposition of nerve tissue for peripheral nerve defects. J Reconstr Microsurg 1995;11(1):21–6.
[8] Fansa H, Keilhoff G, Wolf G, Schneider W, Gold BG. Tissue engineering of peripheral nerves: a comparison of venous and acellular muscle grafts with cultured Schwann cells. Plast Reconstr Surg 2001;107(2):495–6.
[9] Yoshii S, Oka M. Collagen filaments as a scaffold for nerve regeneration. J Biomed Mater Res 2001;56(3):400–5.
[10] Yoshii S, Oka M, Shima M, Taniguchi A, Akagi M. Bridging a 30-mm nerve defect using collagen filaments. J Biomed Mater Res A 2003;67(2):467–74.
[11] Yoshii S, Yamamuro T, Ito S, Hayashi M. In vivo guidance of regenerating nerve by laminin-coated filaments. Exp Neurol 1987;96(2):469–73.
[12] Lolley RD, Bose WJ, Bastian F, Bassam B, Meyer FN, Anderson LD. Vein, silastic, and polyglycolic acid fine mesh: a comparative study in peripheral nerve repair. Ann Plast Surg 1995;35(3):266–71.
[13] Terris DJ, Cheng ET, Utley DS, Tarn DM, Ho PR, Verity AN. Functional recovery following nerve injury and repair by silicon tubulization: comparison of laminin–fibronectin, dialyzed plasma, collagen gel, and phosphate buffered solution. Auris Nasus Larynx 1999;26(2):117–22.
[14] Weber RA, Breidenbach WC, Brown RE, Jabaley ME, Mass DP. A randomized prospective study of polyglycolic acid conduits for digital nerve reconstruction in humans. Plast Reconstr Surg 2000;106(5):1036–45. Discussion 46–48.
[15] Dahlin LB, Anagnostaki L, Lundborg G. Tissue response to silicone tubes used to repair human median and ulnar nerves. Scand J Plast Reconstr Surg Hand Surg 2001;35(1):29–34.
[16] Millesi H, Meissl G, Berger A. The interfascicular nerve-grafting of the median and ulnar nerves. J Bone Joint Surg Am 1972;54(4):727–50.
[17] Millesi H, Meissl G, Berger A. Further experience with interfascicular grafting of the median, ulnar, and radial nerves. J Bone Joint Surg Am 1976;58(2):209–18.
[18] Belkas JS, Shoichet MS, Midha R. Peripheral nerve regeneration through guidance tubes. Neurol Res 2004;26(2):151–60.
[19] Chaudhry V, Glass JD, Griffin JW. Wallerian degeneration in peripheral nerve disease. Neurol Clin 1992;10(3):613–27.
[20] Morris JH, Hudson AR, Weddell G. A study of degeneration and regeneration in the divided rat sciatic nerve based on electron microscopy. I. The traumatic degeneration of myelin in the proximal stump of the divided nerve. Z Zellforsch Mikrosk Anat 1972;124(1):76–102.
[21] Ide C, Tohyama K, Yokota R, Nitatori T, Onodera S. Schwann cell basal lamina and nerve regeneration. Brain Res 1983;288(1–2):61–75.
[22] Itoh S, Takakuda K, Samejima H, Ohta T, Shinomiya K, Ichinose S. Synthetic collagen fibers coated with a synthetic peptide containing the YIGSR sequence of laminin to promote peripheral nerve regeneration in vivo. J Mater Sci Mater Med 1999;10(3):129–34.
[23] Yoshii S, Shima M, Oka M, Taniguchi A, Taki Y, Akagi M. Nerve regeneration along collagen filament and the presence of distal nerve stump. Neurol Res 2004;26(2):145–50.
[24] Bozkurt A, Brook GA, Moellers S, Lassner F, Sellhaus B, Weis J, et al. In vitro assessment of axonal growth using dorsal root ganglia explants in a novel three-dimensional collagen matrix. Tissue Eng 2007;13(12):2971–9.
[25] Olde Damink LH, Dijkstra PJ, van Luyn MJ, van Wachem PB, Nieuwenhuis P, Feijen J. Cross-linking of dermal sheep collagen using a water-soluble carbodiimide. Biomaterials 1996;17(8):765–73.
[26] Kroehne V, Heschel I, Schugner F, Lasrich D, Bartsch JW, Jockusch H. Use of a novel collagen matrix with oriented pore structure for muscle cell differentiation in cell culture and in grafts. J Cell Mol Med 2008.
[27] Vroemen M, Weidner N. Purification of Schwann cells by selection of p75 low affinity nerve growth factor receptor expressing cells from adult peripheral nerve. J Neurosci Methods 2003;124(2):135–43.
[28] Casella GT, Bunge RP, Wood PM. Improved method for harvesting human Schwann cells from mature peripheral nerve and expansion in vitro. Glia 1996;17(4):327–38.
[29] Bowe B, Toal V. White light interferometric surface profiler. Opt Eng 1998;37:1796–9.
[30] Wen X, Tresco PA. Effect of filament diameter and extracellular matrix molecule precoating on neurite outgrowth and Schwann cell behavior on multifilament entubulation bridging device in vitro. J Biomed Mater Res A 2006;76(3):626–37.
[31] IJkema-Paassen J, Jansen K, Gramsbergen A, Meek MF. Transection of peripheral nerves, bridging strategies and effect evaluation. Biomaterials 2004;25(9):1583–92.
[32] Vleggeert-Lankamp CL, de Ruiter GC, Wolfs JF, Pego AP, van den Berg RJ, Feirabend HK, et al. Pores in synthetic nerve conduits are beneficial to regeneration. J Biomed Mater Res A 2007;80(4):965–82.
[33] Fansa H, Keilhoff G, Forster G, Seidel B, Wolf G, Schneider W. Acellular muscle with Schwann-cell implantation: an alternative biologic nerve conduit. J Reconstr Microsurg 1999;15(7):531–7.
[34] Lundborg G. Nerve injury and repair. Churchill Livingstone Inc.; 1988.
[35] Stang F, Fansa H, Wolf G, Reppin M, Keilhoff G. Structural parameters of collagen nerve grafts influence peripheral nerve regeneration. Biomaterials 2005;26(16):3083–91.
[36] Keilhoff G, Stang F, Wolf G, Fansa H. Bio-compatibility of type I/III collagen matrix for peripheral nerve reconstruction. Biomaterials 2003;24(16):2779–87.
[37] Millesi H, Terzis JK. Nomenclature in peripheral nerve surgery. Committee report of the International Society of Reconstructive Microsurgery. Clin Plast Surg 1984;11(1):3–8.
[38] Lietz M, Dreesmann L, Hoss M, Oberhoffner S, Schlosshauer B. Neuro tissue engineering of glial nerve guides and the impact of different cell types. Biomaterials 2006;27(8):1425–36.
[39] Goldner JS, Bruder JM, Li G, Gazzola D, Hoffman-Kim D. Neurite bridging across micropatterned grooves. Biomaterials 2006;27(3):460–72.
[40] Mahoney MJ, Chen RR, Tan J, Saltzman WM. The influence of microchannels on neurite growth and architecture. Biomaterials 2005;26(7):771–8.
[41] Noah EM, Chen J, Jiao X, Heschel I, Pallua N. Impact of sterilization on the porous design and cell behavior in collagen sponges prepared for tissue engineering. Biomaterials 2002;23(14):2855–61.
[42] Ahmed MR, Venkateshwarlu U, Jayakumar R. Multilayered peptide incorporated collagen tubules for peripheral nerve repair. Biomaterials 2004;25(13):2585–94.
[43] Harley BA, Hastings AZ, Yannas IV, Sannino A. Fabricating tubular scaffolds with a radial pore size gradient by a spinning technique. Biomaterials 2006;27(6):866–74.
[44] Itoh S, Takakuda K, Kawabata S, Aso Y, Kasai K, Itoh H, et al. Evaluation of cross-linking procedures of collagen tubes used in peripheral nerve repair. Biomaterials 2002;23(23):4475–81.
[45] Moore MJ, Friedman JA, Lewellyn EB, Mantila SM, Krych AJ, Ameenuddin S, et al. Multiple-channel scaffolds to promote spinal cord axon regeneration. Biomaterials 2006;27(3):419–29.
[46] Ahmed MR, Vairamuthu S, Shafiuzama M, Basha SH, Jayakumar R. Microwave irradiated collagen tubes as a better matrix for peripheral nerve regeneration. Brain Res 2005;1046(1–2):55–67.
[47] Torigoe K, Tanaka HF, Takahashi A, Awaya A, Hashimoto K. Basic behavior of migratory Schwann cells in peripheral nerve regeneration. Exp Neurol 1996;137(2):301–8.
[48] Thompson DM, Buettner HM. Neurite outgrowth is directed by Schwann cell alignment in the absence of other guidance cues. Ann Biomed Eng 2006;34(1):161–8.
[49] Shibuya Y, Mizoguchi A, Takeichi M, Shimada K, Ide C. Localization of N-cadherin in the normal and regenerating nerve fibers of the chicken peripheral nervous system. Neuroscience 1995;67(1):253–61.
[50] Zhang Y, Roslan R, Lang D, Schachner M, Lieberman AR, Anderson PN. Expression of CHL1 and L1 by neurons and glia following sciatic nerve and dorsal root injury. Mol Cell Neurosci 2000;16(1):71–86.
[51] Thornton MR, Mantovani C, Birchall MA, Terenghi G. Quantification of N-CAM and N-cadherin expression in axotomized and crushed rat sciatic nerve. J Anat 2005;206(1):69–78.
[52] Heumann R, Korsching S, Bandtlow C, Thoenen H. Changes of nerve growth factor synthesis in nonneuronal cells in response to sciatic nerve transection. J Cell Biol 1987;104(6):1623–31.
[53] Smith GM, Rabinovsky ED, McManaman JL, Shine HD. Temporal and spatial expression of ciliary neurotrophic factor after peripheral nerve injury. Exp Neurol 1993;121(2):239–47.
[54] Bradley WG, Asbury AK. Duration of synthesis phase in neuilemma cells in mouse sciatic nerve during degeneration. Exp Neurol 1970;26(2):275–82.
[55] Son YJ, Thompson WJ. Schwann cell processes guide regeneration of peripheral axons. Neuron 1995;14(1):125–32.
[56] Ann ES, Mizoguchi A, Okajima S, Ide C. Motor axon terminal regeneration as studied by protein gene product 9.5 immunohistochemistry in the rat. Arch Histol Cytol 1994;57(4):317–30.
[57] Hadlock T, Sundback C, Hunter D, Cheney M, Vacanti JP. A polymer foam conduit seeded with Schwann cells promotes guided peripheral nerve regeneration. Tissue Eng 2000;6(2):119–27.
[58] Evans GR, Brandt K, Katz S, Chauvin P, Otto L, Bogle M, et al. Bioactive poly(L-lactic acid) conduits seeded with Schwann cells for peripheral nerve regeneration. Biomaterials 2002;23(3):841–8.
[59] Mosahebi A, Fuller P, Wiberg M, Terenghi G. Effect of allogeneic Schwann cell transplantation on peripheral nerve regeneration. Exp Neurol 2002;173(2):213–23.
[60] Sinis N, Schaller HE, Schulte-Eversum C, Schlosshauer B, Doser M, Dietz K, et al. Nerve regeneration across a 2-cm gap in the rat median nerve using a resorbable nerve conduit filled with Schwann cells. J Neurosurg 2005;103(6):1067–76.